Surface & Coatings Technology 406 (2021) 126666

Contents lists available at ScienceDirect

Surface & Coatings Technology

journal homepage: www.elsevier.com/locate/surfcoat

The effect of the substrate surface state on the morphology, topography and tribocorrosion behavior of Si/Zr sol-gel coated 316L stainless steel

Stephania Kossman [a,*], Leonardo Bertolucci Coelho [b], Alex Montagne [a], Alberto Mejias [a,c], Adrien Van Gorp [a], Thierry Coorevits [a], Matthieu Touzin [d], Marie-Eve Druart [e], Mariana H. Staia [a,f], Marc Poorteman [b], Marie-Georges Olivier [b,e]

[a] Arts et Métiers Institute of Technology, MSMP, HESAM Université, F-59000 Lille, France
[b] Department of Materials Science, Faculty of Engineering, University of Mons, 7000 Mons, Belgium
[c] Université de Lille, IUT-A, Département GMP, F-59650 Villeneuve d'Ascq, France
[d] Univ. Lille, CNRS, INRAE, Centrale Lille, UMR 8207 - UMET - Unité Matériaux et Transformations, F-59000 Lille, France
[e] Materia Nova asbl, Avenue Copernic 1, 7000 Mons, Belgium
[f] Escuela de Ingeniería y Ciencia de los Materiales, Facultad de Ingeniería, Universidad Central de Venezuela, Caracas 1041, Venezuela

ARTICLE INFO

Keywords:
Sol-gel coatings
Morphology
Topography
Tribocorrosion
Stainless steel

ABSTRACT

In the present work, a Si/Zr based sol–gel (SG) coating was deposited on 316L stainless steel plates, previously treated by passivation (SSO) or electropolishing (SSEP) producing two different surface states. The SG coatings were compared for SSO and SSEP substrates in terms of morphology, topography and tribocorrosion response. The coating topography revealed a smoother surface for the Si/Zr-SSEP system. The coating deposited on the smoothest surface (Si/Zr-SSEP) presented half of the thickness of the one deposited on the roughest surface (Si/Zr-SSO). Tribocorrosion behavior was studied under potentiostatic control at anodic potential with a continuous recording of current (*I*) during sliding (pin-on-disc and alumina ball counterbody). Both SG systems showed an increase of current upon 100 sliding contact cycles indicating corrosion activity. After tribocorrosion tests, both systems revealed scratches, typical of abrasion, and coating removal in the wear tracks; the alumina counterparts presented accumulation of wear particles adhered to their surfaces. In conclusion, the initial surface state of the substrate modified the coating thickness, topography but did not significantly alter the tribocorrosion response of the studied SG systems.

1. Introduction

The development of sol–gel (SG) technologies for surface functionalization (i.e. corrosion protection) has been of interest within the last decades due to its low environmental imprint and its easy-to-depose process. Indeed, the sol–gel method allows the control of the chemical composition/microstructure of the film at a great extent, while remaining of simple employment and based on low-cost equipment [1]. The sol–gel process is considered as a green technology since in comparison with other classic coating deposition techniques: (i) the processing temperature is usually low, (ii) it does not introduce impurities in the final material, (iii) waste is minimized, (iv) the final pieces do not need a washing step [2,3]. The sol–gel route has allowed the production of a wide variety of ceramic and hybrid coatings with tailored composition and has thus offered great opportunities for industrial applications; namely optical sensors, thermal barriers, anticorrosion, electrochemical and wear protection [4]. For instance, oxide coatings developed via sol–gel have been employed in tribological applications, thanks to its excellent anti-wear and friction performance under low loads [4,5]. Concerning hybrid coatings, these are extensively used due to the possibility of combining properties related to polymer and ceramic materials, often resulting in enhanced adhesion and surface coverage [4,6]. Nonetheless, this type of sol–gel coating is still not extensively used for tribological applications due to their poor fracture toughness [4].

Interest has been paid to the SiO_2/ZrO_2 system due to its appealing properties, such as high hardness and chemical and wear resistance [7]. Zirconium oxides have also been applied as interlayers (interface between the substrate and other layers), in sol–gel materials. An advantage associated with this oxide is the large number of Van der Waals bonds

* Corresponding author.
E-mail address: stephaniakossman@gmail.com (S. Kossman).

https://doi.org/10.1016/j.surfcoat.2020.126666
Received 25 August 2020; Received in revised form 16 November 2020; Accepted 19 November 2020
Available online 20 November 2020

that form with the metallic substrates, which might be transformed into stronger covalent bonds upon heat treatment [8]. According to Neacşu et al., sol–gel films containing ZrO_2 deposited on metals have resulted in improved resistance to corrosion and wear [1].

Today a real challenge is to optimize the sol–gel systems (substrate and sol–gel formulation) to work properly under the combined action of several solicitations, for example, wear and corrosion (tribocorrosion) to fulfil their technical functions in the long term. Tribocorrosion degradation is a primary concern in various fields, such as mining, transport, food, nuclear, offshore, marine, and biomedical. Indeed, erosion-corrosion is a typical process of coating failure often encountered in pumps, impellers, propellers, valves, heat exchanger tubes and other fluid-handling equipment [9,10].

The substrate surface plays a critical role on the resulting properties of coated systems (not being an exception for sol–gel coatings), affecting their topographical characteristics, including surface roughness, and their performance in service. Nevertheless, this subject has not been extensively addressed in the literature [11]. Moreover, the surface pre-treatment of the substrates modifies the integrity, homogeneity, and adhesion of the coating [11].

Therefore, this work evaluated the influence of two industrially treated 316L stainless steel surfaces (passivated and electropolished) on the morphology, topography and tribocorrosion behavior of Si/Zr based sol–gel coatings.

316L industrial surfaces were chosen as substrates since they are largely used due to their mechanical strength and high corrosion resistance. Nevertheless, these materials do not resist well to tribocorrosion solicitations, where mechanical perturbations of the passive layer might yield to more aggressive corrosion mechanisms. Sol–gel coatings represent a green alternative to improve tribocorrosion properties and enhance the material durability in service.

The tribocorrosion performance was previously studied under potentiostatic anodic polarization in the passivity range of the stainless steel substrates [12]. In this method, the anodic current is monitored while applying a constant anodic potential before, during and after the sliding, which is a well-established approach [13,14]. Tribocorrosion characterization of sol–gel films is a research topic not broadly covered in the literature yet.

2. Materials and methods

2.1. Materials

2.1.1. Substrates

The substrates for the sol–gel coatings were 316L stainless steel (SS) plates (Aperam, France) treated by two different industrial surface treatments (Packo Inox NV, Belgium): (1) chemical passivation, named SSO; and (2) electropolishing followed by passivation, named SSEP. The initial surface state of all plates was 2B surface finish [15,16]. The substrates and corresponding nomenclature were employed in previous investigations of the authors [12,14]. The bulk composition of the 316L plates was in wt%: Cr 17.3, Ni 10.1, Mo 2.2, Cu 0.5, Mn 0.3, Si 0.2, C 0.02–0.03, Fe balance [12]. The passive layer of SSEP substrate presented chromium enrichment compared to the SSO surfaces [12].

Before sol–gel application, the 316L substrates were first degreased in acetone using an ultrasonic bath (15 min), rinsed with ethanol, dried with compressed air, and then degreased using Gardoclean G-C S5117 (50 °C).

2.1.2. Sol–gel coatings

The Si/Zr SG was obtained by mixing Si-based and Zr-based solutions individually prepared. First, an organosilane solution was prepared by mixing tetraethylorthosilicate (TEOS), 3-glycidyloxypropyl-trimethoxysilane (GPTMS), methyltriethoxysilane (MTES) in an equal weight percentage. The Si-based solution contains 10%, 70%, and 20% wt. of precursors, water, and ethanol, respectively. The pH was adjusted at approximately 3 by adding concentrated acetic acid. After stirring for 40 min, a dispersant agent (Pluronic® F108) was added to improve the wettability, and the solution was left under vigorous stirring for 40 min at room temperature.

In parallel, a Zr-based sol was prepared by mixing zirconium butoxide ($Zr(OC_4H_9)_4$) with propanol and acetylacetonate in the following proportions 45/46.5/8.5% wt, respectively (1 h of stirring in a dark room). Finally, the Si-based and Zr-based sols were mixed up under continuous stirring, and the final solution has a Si/Zr molar ratio equal to 3.2. The pH of the sol was adjusted to 2.5 upon addition of nitric acid and left to hydrolyze for 24 h (room temperature). All the reagents were either purchased from Sigma-Aldrich or Merck and used as received without further purification. Then, the prepared 316L substrates were coated with the hybrid organic–inorganic sol–gel layer using a KSV Nima dip-coater in a deposition chamber at room temperature (2 min of immersion, a withdrawal rate of 100 mm/min). Next, curing was carried out at 270 °C for 1 h in a furnace with no controlled atmosphere, yielding uniform and transparent coatings. The used nomenclature for the coated systems is Si/Zr-SSO and Si/Zr-SSEP.

2.2. Coating characterization methodology

2.2.1. Morphology characterization

Coating surfaces and cross-sections were evaluated by scanning electron microscopy SEM coupled with energy-dispersive X-ray spectroscopy (EDS) (JEOL JSM-7800F LV, Japan). Grazing incidence X-ray diffraction (GIXD) analysis for crystallographic analysis was performed using a Siemens D5000 diffractometer in grazing incidence geometry (0.2) with a Cu Ka radiation.

2.2.2. Topography characterization

The surface morphology was characterized by contact profilometry (P16-KLA-Tencor, USA) using a diamond stylus (cone of 60° angle and a 2 μm tip radius): sixteen profiles spaced of 1 mm and 8 mm length with a 10 nm vertical resolution and about 0.1 μm in lateral resolution. The measurements were carried out perpendicular and parallel to the direction of the coating deposition (dip-coating) and on the bare substrates for comparison.

The surface data were analyzed by a multiscale approach [17] to determine the scale of pertinence at which the surfaces can be distinguished between them. The next parameters were calculated for the evaluation length according to the ISO 4287 standard: *R*a (arithmetical mean deviation of the profile), *R*v (maximum profile valley depth), *R*t (total height profile).

2.2.3. Tribocorrosion tests

The tribocorrosion tests were carried out under potentiostatic control at anodic potential (E_a = +200 mV vs $Ag/AgCl/KCl_{sat}$) corresponding to the passivity ranges of the studied substrates, selected from a potentiodynamic polarization presented in a previous study [12]. Corrosion and mechanical wear assessment are described here below. All the tests were performed at room temperature. Two tribocorrosion tests were performed for each type of system.

Corrosion measurements were performed using a three-electrode configuration: the coated systems Si/Zr-316L as working electrode (WE) (exposed area of 1.76 cm^2 properly isolated), a Pt-wire auxiliary electrode and an $Ag/AgCl/KCl_{sat}$ as a reference electrode (RE). The electrolyte was 0.5 M NaCl, and its volume was maintained constant (35 ml) for all experiments. The corrosion measurements were done using a potentiostat/galvanostat Solartron 1287 (Ametek, USA). Details of the tribocorrosion cell are given in previous work [14].

Wear measurements during tribocorrosion tests were conducted in a pin-on-disc tribometer TRIBOtester (Tribotechnic, France) using an inert alumina ball (10 mm diameter, grade 25, ISO 3290) as the counterpart. The tests were carried out at 1 N normal load. The sliding rate and distance were 12.6 mm/s (60 rpm) and 10 m (equivalent to

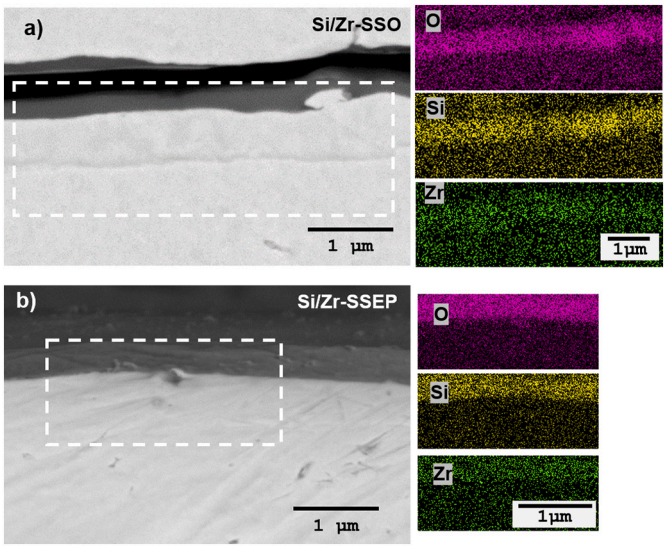

Fig. 1. SEM-EDS analysis of the cross-sections of (a) Si/Zr-SSO and (b) Si/Zr-SSEP systems.

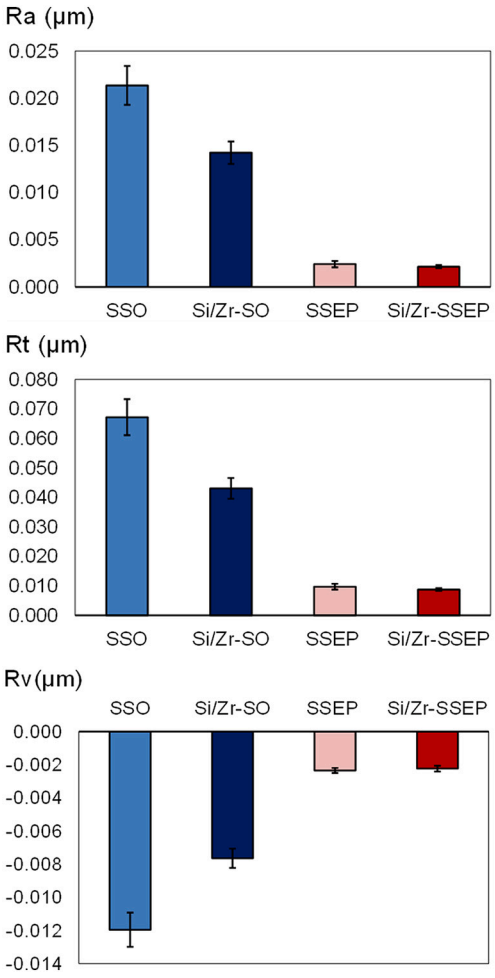

Fig. 2. Morphology multi-scale analysis results, showing roughness parameters *Ra*, *Rt* and *Rv* comparing coated and uncoated surfaces. The scale of pertinency [17] was approximately 2 µm for these parameters.

approximately 800 cycles), respectively, using a wear track radius of 2 mm. The contact interval time was 1000 ms. During the tribocorrosion tests, the current (*I*) and the coefficient of friction (COF) were recorded simultaneously.

2.2.4. Surface analysis after tribocorrosion

The characterization of wear tracks was performed by scanning electron microscopy SEM coupled with energy-dispersive X-ray spectroscopy (EDS) (JEOL JSM-7800F LV, Japan) and contact profilometry (P16-KLA-Tencor, USA). The alumina balls counterparts were characterized by optical microscopy (Keyence VHX-7000, Japan) and profilometry (Veeco NT-9300, USA) after tribocorrosion tests.

The wear-corrosion volumes were estimated from contact profilometry measurements of the wear tracks done in four locations along their perimeter. Then, the average cross-section area obtained from the measured profiles was multiplied by the nominal wear track perimeter to estimate the tribocorrosion volume lost.

3. Results and discussion

3.1. Coating characterization

SEM analysis using in secondary electron mode from the top-surfaces of the sol–gel/316L systems demonstrated the dense and uniform aspect of the coatings for both systems (images not displayed). SEM analysis from the cross-sections (Fig. 1) allowed to verify that coatings were highly covering on both SSO and SSEP substrates, explained by the SiOH and ZrOH groups appearing during hydrolysis, which are adsorbed onto the metal surface through hydrogen bonds and form during drying and curing covalent bonds (MeOSi or MeOZr) from the metal surface [18]. Moreover, by image analysis, an estimation of the coating thicknesses was obtained: 598 ± 45 nm and 319 ± 12 nm for the sol–gel films on SSO and SSEP, respectively.

GIXD analysis carried out on sol–gel/316L systems highlighted the amorphous microstructure of the coatings (results not displayed). Indeed, no crystallization of the sol–gel network was expected after heat treatment at 270 °C [19].

3.2. Topography of coated surfaces

Fig. 2 shows the roughness parameters (*Ra*, *Rt* and *Rv*) obtained by the multi-scale analysis [17] for a comparison between coated systems and substrates evaluated at a scale of pertinency of 2 µm. The surface topography did not change with the measuring direction suggesting isotropic surfaces for both systems. These results indicated that surface roughness was more significant for the Si/Zr-SSO system regardless of the roughness parameter (*Ra* and *Rt* parameters were one order of magnitude greater than Si/Zr-SSEP).

Moreover, the multi-scale analysis revealed that the deposition of the sol–gel produced a different effect according to the type of substrate. Indeed, in the case of the Si/Zr-SSO system, the coating produced a general diminution of surface roughness with respect to the SSO substrate (decrease of *Ra* of approximately 33%), giving a smoothening effect to the initial surface. In other words, the coating covered the surface topography of SSO. It partially filled the valleys, which was expressed by an apparent reduction of the roughness parameters *Rv* and *Rt* of about 35% with respect to SSO substrate (Fig. 2).

Conversely, the deposition of the coating on the SSEP substrate did not produce significant changes with respect to the initial surface. In this case, the coating instead replicated the substrate topography. Therefore, the roughness parameters of coated and uncoated surfaces remained very similar (Fig. 2). The differences between the topography of both surfaces could justify the resulting thickness variation between them [20,21].

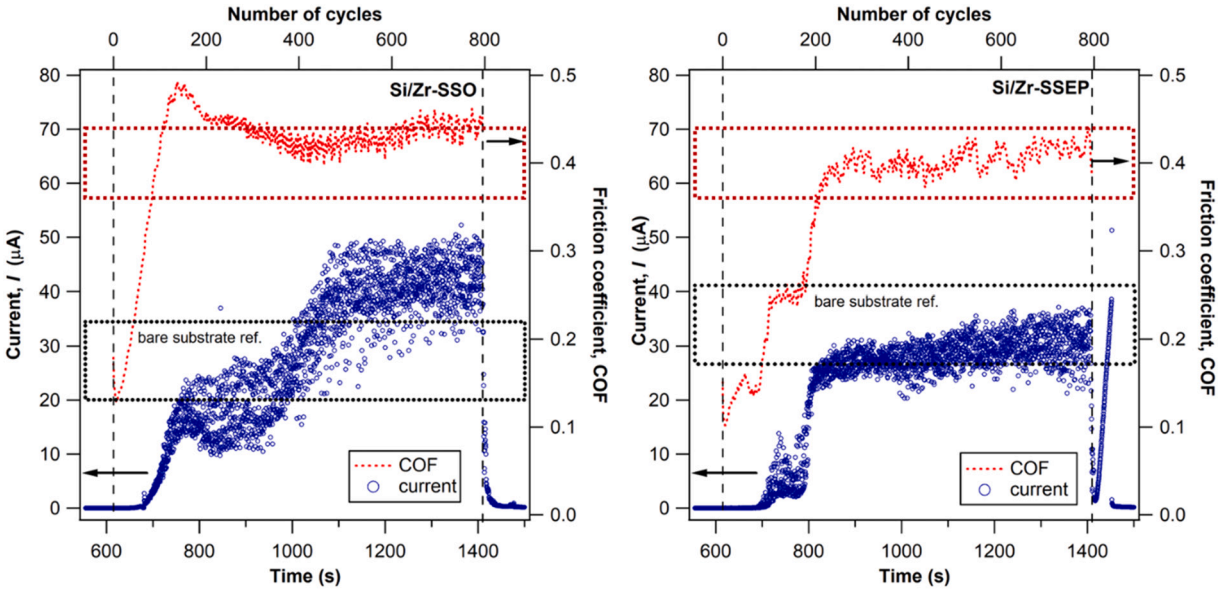

Fig. 3. Current and friction coefficient as a function of time (number of cycles). The regions delimited by the dotted lines correspond to the ranges of current and COF values for the bare substrates under similar testing conditions [14].

3.3. Tribocorrosion

The tribocorrosion response (COF and current) of the Si/Zr sol–gel coatings under potentiostatic anodic control (+200 mV vs Ag/AgCl) are presented in Fig. 3. For simplicity only one representative test per sample is shown since duplicate tests produced very similar results. The following results and discussion described below, represent the two tests per system. Before the sliding action, both systems showed relatively low current values (even negative ones, typically about -10^{-2} μA), which indicated the coating barrier effect (i.e. no corrosion) and good surface coverage for both systems. Upon sliding, the current magnitudes remained very small (<+1 μA) until approximately 100 cycles, hence still indicating the coating barrier effect. After this phase, a sudden rise of the current was observed, signaling the initial failure of the coating (e.g. cracking), although the response differed slightly depending on the substrate. Finally, when the current reached the substrate reference values: 28 ± 8 μA for SSO and SSEP 35 ± 8 μA (according to results in [14]) (region delimited by dotted lines in Fig. 3), it indicated that the

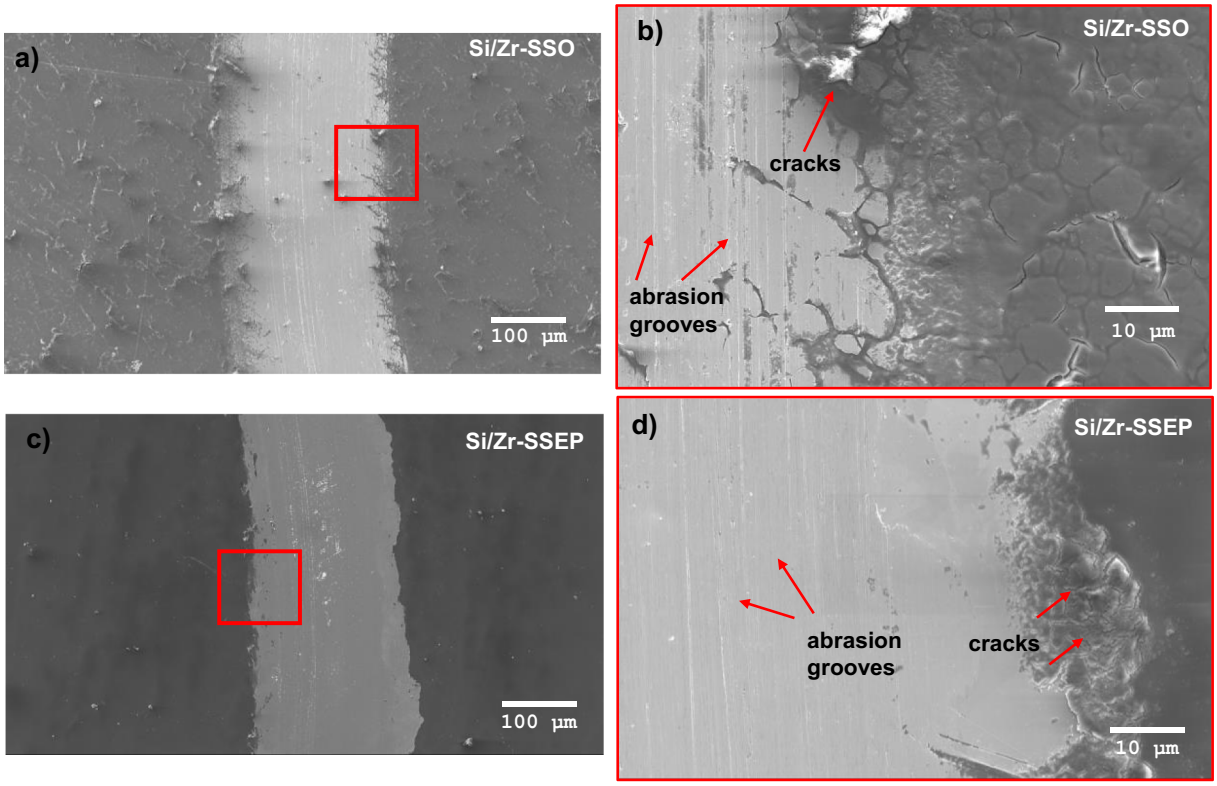

Fig. 4. SEM micrographs (secondary electron mode) of wear tracks after tribocorrosion tests under potentiostatic control (+200 mV vs. Ag/AgCl/KCl_{sat}): a–b) Si/Zr-SSO, c–d) Si/Zr-SSEP.

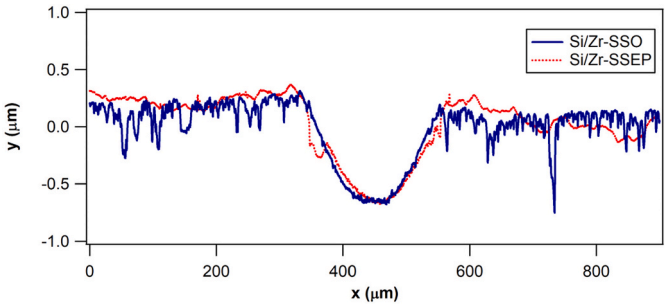

Fig. 5. Wear track profiles obtained by contact profilometry for SG Si/Zr-stainless steel samples after tribocorrosion tests.

tribological contact arrived to the substrate, consequently exposing it to the electrolyte. From Benea et al. [22] observations, an increase of the anodic current upon application of anodic potential seems to be the result of a low oxide growth rate compared with the frequency of the mechanical depassivation caused by the friction. Once the sliding stopped, the current values rapidly decreased, indicating repassivation of the worn areas [13,22].

The COF evolution displayed a run-in period of about 100 (SSEP) or 200 (SSO) cycles. For the Si/Zr-SSO system, the sharper change (from 0.1 to 0.5) during this period, was related to the smoothing of asperities associated to the higher surface roughness. After this period, friction coefficient modifications were associated to coating thinning and production of third body (sol–gel and metallic) particles. These particles could remain trapped within the contact, producing more damage, eventually leading to the elimination of the coating from the contact zone. At the final stage of contact sliding, the COF tended to a steady-state, and the values were analogous to the reference values for the bare substrates (~0.4) [14], most likely indicating that the coating had no interference at the contact anymore. Consequently, the 10 m sliding distance was adequate to study the tribocorrosion response of the coated systems.

It is worth mentioning that the friction coefficient and current evolution seemed to be closely related during sliding in both systems. The surfaces in contact evolved with the number of cycles and so the COF and current. Namely, producing simultaneous changes in the electrochemical and mechanical responses, reinforcing the notion of complexity of tribocorrosion mechanisms. A clear example was the

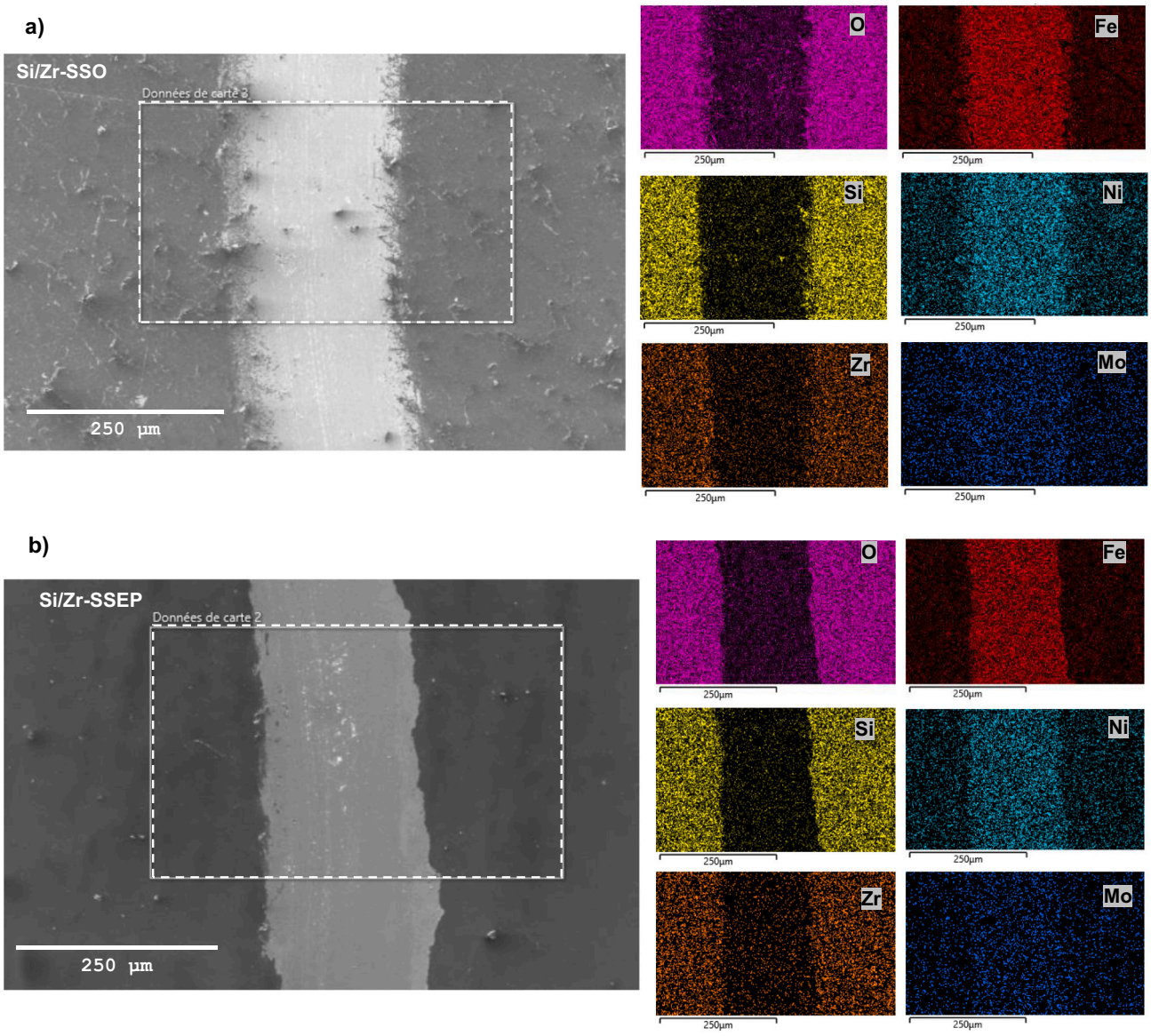

Fig. 6. SEM-EDS analysis of wear tracks after tribocorrosion tests: a) Si/Zr-SSO system, b) Si/Zr-SSEP.

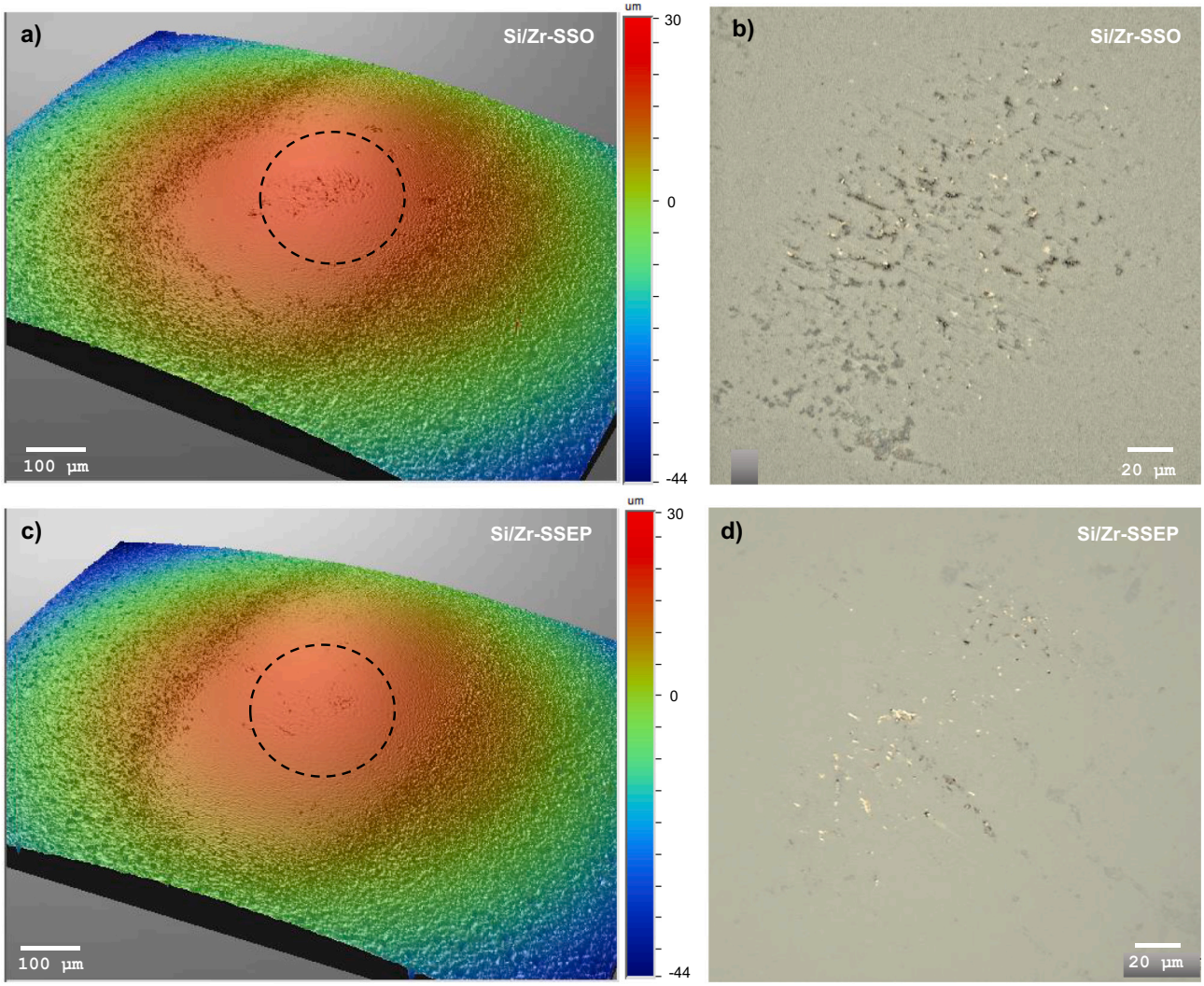

Fig. 7. 3D Optical profilometry analysis (a,c) and 2D optical microscopy images (b,d) of alumina balls after tribocorrosion tests. Optical microscopy images correspond to regions inside the circles in the profilometry analysis.

increase of the current that indicated coating removal and depassivation (active corrosion) of 316L substrate. In this study, both parameters (current and COF) increased with the sliding distance, revealing the final contact substrate/counterbody at the end of the tests. This behavior was somehow analogous to the one observed during tribocorrosion tests under potentiodynamic scan described by Chen et al. [23]. A clear correlation between the current and COF evolutions was particularly identified for Si/Zr-SSEP upon sliding.

3.3.1. *Tribocorrosion mechanisms*

SEM analysis of the wear tracks presented in Fig. 4 revealed scratches on their surfaces, signaling abrasion as the main mechanism for both studied systems. The continuous sliding action probably produced cracking of the coating due to the hard counterbody, leading to the formation of third-body particles and, finally, to the removal of the coating from the contact zone. The characteristic microstructures of the substrates [12] were observed in both systems at the edges of the wear tracks, revealing that the substrates were reached during sliding, as expected according to the current and friction coefficient values by the end of the tests.

Analysis of the wear track profiles (Fig. 5) showed a comparable behavior for both systems, which was also reflected by the similar estimated wear-corrosion volumes (Si/Zr-SSO: 1.2 ± 0.2 [10^{-3} mm^3], Si/Zr-SSEP: 1.1 ± 0.2 [10^{-3} mm^3]), despite the difference between coating thicknesses. These results suggested that the Si/Zr-SSO surface (higher roughness and thickness) presented more limited mechanical strength in comparison to the Si/Zr-SSEP surface, and consequently produced a higher amount of debris. During testing, however, both coatings suffered cracking and delamination while the substrates were plastically deformed, finally being removed from the contact zones. Namely, after coating removal the tribocorrosion response of both substrates remained similar, and the coating only affected the initial response.

The SEM (integrated with EDS) analysis of the wear tracks presented in Fig. 6 shows that, in both systems, the SG coating was significantly removed from the contact zone after sliding, suggested by the contrast of Si and Zr elements between regions inside and outside the wear tracks, corroborating the previously described results (*I* and *COF*).

The alumina counterparts did not present damage on their surfaces after tribocorrosion tests. Nonetheless, wear debris accumulation (mainly coating debris) formed a groove-like pattern (Fig. 7) alike to the morphology of abrasion wear tracks (Fig. 4). It could be qualitatively inferred that higher amounts of debris remained attached to the counterbody after testing with the SSO system (in comparison to the SSEP system).

4. Discussion

On the one hand, as discussed in the previous results the general tribocorrosion behavior of the sol–gel/316L systems were not significantly affected by the substrate surface state, the small differences among both surfaces were likely related to the tests reproducibility. Moreover, tribocorrosion assessment indicated that the Si/Zr coating protected the 316L surfaces for a short period (approximately 100 s = 100 cycles) under the studied wear-corrosion conditions, then, the coatings were removed from the contact surfaces, and mechanical depassivation occurred in the 316L surfaces.

On the other hand, the substrate topography played an essential role during coating deposition, modifying its thickness and topography, which might have affected the corrosion and wear response of sol–gel systems in a minor level, although undetectable under the studied conditions, which produced a similar output for both surfaces. Ideally for tribocorrosion comparison, coatings should have had similar thicknesses. However, this investigation was focused on the study of the substrate surface effect on the resulting sol–gel coatings and tribocorrosion behavior. To achieve similar thicknesses for both substrates the deposition process would have need to be modified.

It is worth mentioning that a higher surface roughness for the system Si/Zr-SSO might produce a detrimental effect in the coating and tribocorrosion response according to previous investigations. Nofz et al. [11] mentioned that the substrate surface pretreatment modifies the integrity, homogeneity and adhesion of the coating, also pointing out that the coating thickness and depth of valleys intervene in the formation of local defects in the coating. Many authors have reported that higher roughness could be responsible for a negative response in the corrosion [24–26] and wear [27–30] behavior. However, in the current study, this negative response in tribocorrosion conditions was not observed and could be subject to further investigations using different coating formulations.

5. Conclusions

- The Si/Zr sol–gel coating showed an excellent surface coverage indistinctly of the 316L surface state.
- The surface state of the 316L substrate affected the thickness of Si/Zr sol–gel coatings, with the smoothest surface (SSEP) presenting half of the thickness (about 320 nm) of the estimation for the roughest surface (SSO).
- The final Si/Zr sol–gel topography depends on the underneath surface. The coating produces a smoothing effect on rougher surfaces such as SSO, notably filling the valleys of the topography, reducing approximately by 30% the roughness parameters. For smoother surfaces (SSEP), the sol–gel coating replicated the surface topography.
- The tribocorrosion behavior of the sol–gel/316L coated systems were not affected by the substrate topography under the studied conditions.

Funding

This work was supported by the Interreg France-Wallonie-Vlaanderen program, TRANSPORT, with the financial support of the European Regional Development Fund (ERDF) and Walloon Region.

CRediT authorship contribution statement

Stephania Kossman: Conceptualization, Methodology, Formal analysis, Writing - original draft, Investigation, Validation, Visualization. **Leonardo Bertolucci Coelho:** Conceptualization, Methodology, Validation, Investigation, Writing - original draft, Visualization. **Alex Montagne:** Validation, Writing - review & editing, Project administration, Funding acquisition. **Alberto Mejias:** Conceptualization, Methodology, Validation, Writing - review & editing. **Adrien Van Gorp:** Investigation, Writing - review & editing. **Thierry Coorevits:** Investigation, Writing - review & editing. **Matthieu Touzin:** Investigation. **Marie-Eve Druart:** Investigation, Methodology. **Mariana H. Staia:** Validation, Writing - review & editing, Supervision. **Marc Poorteman:** Writing - review & editing, Project administration, Funding acquisition. **Marie-Georges Olivier:** Validation, Writing - review & editing, Supervision.

Declaration of competing interest

The authors declare that they have no known competing financial interests or personal relationships that could have appeared to influence the work reported in this paper.

Acknowledgements

The authors acknowledge to Packo Inox nv. for providing stainless steel treated plates. The SEM facility in Lille (France) is supported by the Conseil Régional du Nord-Pas de Calais, and the European Regional Development Fund (ERDF).

References

[1] I.A. Neacşu, A.I. Nicoară, O.R. Vasile, B.Ş. Vasile, in: A.M. Grumezescu (Ed.), Chapter 9 - Inorganic Micro- and Nanostructured Implants for Tissue Engineering, William Andrew Publishing, 2016, pp. 271–295, https://doi.org/10.1016/B978-0-323-42862-0.00009-2.
[2] D. Balgude, A. Sabnis, Sol–gel derived hybrid coatings as an environment friendly surface treatment for corrosion protection of metals and their alloys, J. Sol-Gel Sci. Technol. 64 (2012) 124–134, https://doi.org/10.1007/s10971-012-2838-z.
[3] R. Figueira, I. Fontinha, C. Silva, E. Pereira, Hybrid sol-gel coatings: smart and green materials for corrosion mitigation, Coatings 6 (2016) 12, https://doi.org/10.3390/coatings6010012.
[4] S. Rahoui, V. Turq, J.P. Bonino, Effect of thermal treatment on mechanical and tribological properties of hybrid coatings deposited by sol-gel route on stainless steel, Surf. Coatings Technol. 235 (2013) 15–23, https://doi.org/10.1016/j.surfcoat.2013.07.008.
[5] W. Liu, Y. Chen, G.-T. Kou, T. Xu, D.C. Sun, Characterization and mechanical/tribological properties of nano Au–TiO2 composite thin films prepared by a sol–gel process, Wear 254 (2003) 994–1000, https://doi.org/10.1016/S0043-1648(03)00305-3.
[6] J.B. Cambon, F. Ansart, J.P. Bonino, V. Turq, Effect of cerium concentration on corrosion resistance and polymerization of hybrid sol-gel coating on martensitic stainless steel, Prog. Org. Coatings. 75 (2012) 486–493, https://doi.org/10.1016/j.porgcoat.2012.06.005.
[7] Y. Castro, M. Aparicio, R. Moreno, A. Durán, Silica-zirconia sol–gel coatings obtained by different synthesis routes, J. Sol-Gel Sci. Technol. 35 (2005) 41–50, https://doi.org/10.1007/s10971-005-3213-0.
[8] J. Gasiorek, A. Szczurek, B. Babiarczuk, J. Kaleta, W. Jones, J. Krzak, Functionalizable sol-gel silica coatings for corrosion mitigation, Materials (Basel) 11 (2018) 1–18, https://doi.org/10.3390/ma11020197.
[9] A. López-Ortega, J.L. Arana, R. Bayón, Tribocorrosion of passive materials: a review on test procedures and standards, Int. J. Corros. 2018 (2018) 1–24, https://doi.org/10.1155/2018/7345346.
[10] R.J.K. Wood, J.A. Wharton, Coatings for tribocorrosion protection, in: Tribocorrosion Passiv. Met. Coatings, Elsevier, 2011, pp. 296–333, https://doi.org/10.1533/9780857093738.2.296.
[11] M. Nofz, I. Dörfel, R. Sojref, N. Wollschläger, M. Mosquera-Feijoo, A. Kranzmann, Microstructure, smoothening effect, and local defects of alumina sol-gel coatings on ground steel, J. Sol-Gel Sci. Technol. 81 (2017) 185–194, https://doi.org/10.1007/s10971-016-4188-8.
[12] L.B. Coelho, S. Kossman, A. Mejias, X. Noirfalise, A. Montagne, A. Van Gorp, M. Poorteman, M.G. Olivier, Mechanical and corrosion characterization of industrially treated 316L stainless steel surfaces, Surf. Coatings Technol. (2019), https://doi.org/10.1016/j.surfcoat.2019.125175.
[13] S. Hassani, K. Raeissi, M. Azzi, D. Li, M.A. Golozar, J.A. Szpunar, Improving the corrosion and tribocorrosion resistance of Ni-Co nanocrystalline coatings in NaOH solution, Corros. Sci. 51 (2009) 2371–2379, https://doi.org/10.1016/j.corsci.2009.06.026.
[14] S. Kossman, L.B. Coelho, A. Mejias, A. Montagne, A. Van Gorp, T. Coorevits, M. Touzin, M. Poorteman, M.-G. Olivier, A. Iost, M.-H. Staia, Impact of industrially applied surface finishing processes on tribocorrosion performance of 316L stainless steel, Wear (2020), 203341, https://doi.org/10.1016/j.wear.2020.203341.
[15] A01 Committee, ASTM A480 / A480M-18a, Standard Specification for General Requirements for Flat-Rolled Stainless and Heat-Resisting Steel Plate, Sheet, and Strip, West Conshohocken, PA, 2018, https://doi.org/10.1520/A0480_A0480M-18A.

[16] 2B, 2D and cold rolled finishes, (n.d.). https://www.assda.asn.au/technical-info/surface-finishes/2b-2d-and-ba-cold-rolled-finishes (accessed July 29, 2019).
[17] A. Van Gorp, M. Bigerelle, A. Grellier, A. Iost, D. Najjar, A multi-scale approach of roughness measurements: evaluation of the relevant scale, Mater. Sci. Eng. C. 27 (2007) 1434–1438, https://doi.org/10.1016/j.msec.2006.09.041.
[18] D. Zhu, W.J. van Ooij, Corrosion protection of AA 2024-T3 by bis-[3-(triethoxysilyl) propyl]tetrasulfide in sodium chloride solution.Part 2: mechanism for corrosion protection, Corros. Sci. 45 (2003) 2177–2197, https://doi.org/10.1016/S0010-938X(03)00061-1.
[19] D.H. Aguilar, L.C. Torres-Gonzalez, L.M. Torres-Martinez, T. Lopez, P. Quintana, A study of the crystallization of ZrO2 in the sol-gel system: ZrO2-SiO2, J. Solid State Chem. 158 (2001) 349–357, https://doi.org/10.1006/jssc.2001.9126.
[20] C.J. Brinker, G.W. Scherer, Sol-Gel Science: The Physics and Chemistry of Sol-Gel Processing, Gulf Professional Publishing, 1990.
[21] L. Lopez, W.A. Daoud, D. Dutta, B.C. Panther, T.W. Turney, Effect of substrate on surface morphology and photocatalysis of large-scale TiO 2 films, Appl. Surf. Sci. 265 (2013) 162–168, https://doi.org/10.1016/j.apsusc.2012.10.156.
[22] L. Benea, F. Wenger, P. Ponthiaux, J.P. Celis, Tribocorrosion behaviour of Ni-SiC nano-structured composite coatings obtained by electrodeposition, Wear 266 (2009) 398–405, https://doi.org/10.1016/j.wear.2008.04.018.
[23] J. Chen, J. Wang, F. Yan, Q. Zhang, Q.A. Li, Effect of applied potential on the tribocorrosion behaviors of Monel K500 alloy in artificial seawater, Tribol. Int. 81 (2015) 1–8, https://doi.org/10.1016/j.triboint.2014.07.014.
[24] V. Barranco, E. Onofre, M.L. Escudero, M.C. García-Alonso, Characterization of roughness and pitting corrosion of surfaces modified by blasting and thermal oxidation, Surf. Coatings Technol. 204 (2010) 3783–3793, https://doi.org/10.1016/j.surfcoat.2010.04.051.
[25] X. Cheng, S.G. Roscoe, Influence of surface polishing on the electrochemical behavior of titanium, Electrochem. Solid-State Lett. 8 (2005) B38, https://doi.org/10.1149/1.1996509.
[26] G. Ghosh, A. Sidpara, P.P. Bandyopadhyay, Understanding the role of surface roughness on the tribological performance and corrosion resistance of WC-Co coating, Surf. Coatings Technol. 378 (2019), 125080, https://doi.org/10.1016/j.surfcoat.2019.125080.
[27] S.J. Bull, P.R. Chalker, C. Johnston, V. Moore, The effect of roughness on the friction and wear of diamond thin films, Surf. Coatings Technol. 68–69 (1994) 603–610, https://doi.org/10.1016/0257-8972(94)90224-0.
[28] Y. Wan, Z. Xu, W. Chao, J. Zhang, Sol–gel derived nickel-doped TiO2 films as wear protection coatings, J. Exp. Nanosci. 8 (2013) 782–787, https://doi.org/10.1080/17458080.2011.607192.
[29] M. Federici, C. Menapace, A. Moscatelli, S. Gialanella, G. Straffelini, Effect of roughness on the wear behavior of HVOF coatings dry sliding against a friction material, Wear. 368–369 (2016) 326–334, https://doi.org/10.1016/j.wear.2016.10.013.
[30] J.H.W. Siu, L.K.Y. Li, An investigation of the effect of surface roughness and coating thickness on the friction and wear behaviour of a commercial MoS2–metal coating on AISI 400C steel, Wear 237 (2000) 283–287, https://doi.org/10.1016/S0043-1648(99)00349-X.